ELSEVIER

Sensors and Actuators A 93 (2001) 197–205

SENSORS AND ACTUATORS A PHYSICAL

www.elsevier.com/locate/sna

Using fiber gratings in the short-length sensors based on micromechanical vibrations

G.A. Gurchonok, I.A. Djodjua, S.R. Amirova, T.V. Tulaikova*

Moscow Institute of Physics and Technology of Russian Ministry of Education, 9 Institutskii Per., Dolgoprudny, 141700 Moscow, Russia

Received 28 November 2000; received in revised form 12 April 2001; accepted 24 April 2001

Abstract

Fiber-optic inner core gratings are considered together with the non-uniform deformations in oscillated optical-fiber. This is wide method of vibration registration as a result of appropriate deformations. The principle of such new sensors is that the resonance frequency changes under the influence of the environment. Analysis was done for fiber cantilevers with the length 1–10 mm, they vibrate by the photothermally excitation. Different cases were analyzed that correspond to transverse and longitudinal vibrations of the fiber tips or fragments with two clamps. The π-shifted Bragg-gratings and long-period ones are discussed to measure of vibrating amplitude in different real cases.

Keywords: Fiber-optics; Cantilever; Micromechanics; Fiber grating

1. Introduction

The principle of operation of the new class of sensors — micro-optical sensors is considered. Our vibrated fiber cantilevers [1] have convenient inside optical excitation and inner fiber grating in comparison with the predecessor silicon [2] micromechanical vibrated sensor which needs additional optical-fiber with vibrated silicon surface to excite this vibrations which must be permanently adjusted as an interferometer. The typical sizes of these sensors in experiments [1,3] were from 1 up to 30 mm in tip length and from 30 to 125 microns in diameter. Fiber-optic tip (Fig. 1) or fragment (Fig. 2) could be vibrated photothermally by the modulated laser intensity transmission through the optical-fiber, what was proved in experiments [4]. This photothermally vibration excitation was achieved by partial absorption of propagated optical power in additional chromium layer at one side of fiber cylindrical surface. The resonant frequency and Q-factor of vibrated cantilever are output parameters of this sensor, they are sensitive to external parameters such as force, pressure, temperature or medium viscosity and density. If we have narrow response curve then small frequency changes could be measured by fiber sensor, and appropriate small changes in environment as a result. Experimental realization of this sensor is based on the measurements of the response curve. Such measurements were performed in experiment by slow variation of modulated laser frequency. The response curve has maximum of amplitude at the resonant frequency, as this amplitude as Q-factor depends on the environment.

Fiber-optic intercore Bragg-grating have been widely used as a strain sensor [5–7]. The cantilever amplitude is measured by the fiber grating spectrum which depends on non-uniform deformation and strain both in the axial cantilever direction and in the cross-section. For our cases of small tip lengths the maximal values of amplitudes are a few micrometers. It means that the amplitude measurements of the fiber cantilever vibrations must be done reliable and with high accuracy, so the π-shifted grating method for vibration detection of such cantilevers is discussed theoretically to realize a sensitive and convenient measuring of small vibration amplitudes in our cases. Analysis will be done with account of 3D deformation distribution in vibrated fiber fragments. On the other hand, the non-uniform deformation along the fiber core and the cross-section are significally important for the shape of result grating spectrum. Changes in a fiber body influencing to the main grating parameters, such as fiber refractive index, grating coupling coefficient, phase, local deviations of the grating constant and length. In

* Corresponding author. Present address: Institute for Problems in Mechines, Russian Academy of Sciences, 101 Vernadskogo Prosp., 117526 Moscow, Russia. Tel.: +7-95-4085627/5030483; fax: +7-95-4085700/9382048.
E-mail addresses: tulaik@ipmnet.ru, gena@rt.mipt.ru (T.V. Tulaikova).

0924-4247/01/$ – see front matter
PII: S0924-4247(01)00658-6

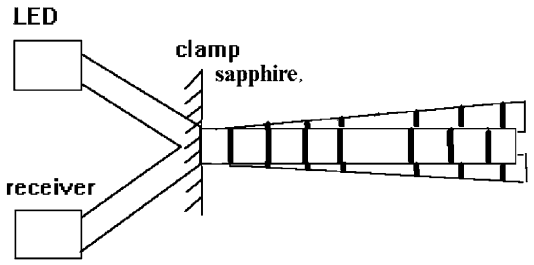

Fig. 1. Bend vibrations of the fiber tip. The quartz fiber core has the grating inside it.

most previous papers [6,7], fiber strain sensors considered as uniform or almost periodical strain functions were used. The method of matrixes approach [8] was modified here to analyze fiber grating vibration with account of the strong non-linear strain. This method based on dividing whole grating into number of segments, and in every one of them the coupled mode equations could be used to describe the contradirectional coupled wave interaction. We introduced the certain modifications based on fiber vibrations effects into the fundamental matrices to each short segment, and the characteristics of whole spectrum was calculated as a result multiplication of these elemental matrices under certain conditions.

The feature of our sensors in this paper is their short lengths of vibrated fiber fragments that means high values of their resonant frequencies (in the range from 1 kHz to 1 MHz). We desire to rise the resonant frequency of our sensors to increase the output sensor sensitivity, so this side of our device sensitivity is the ration of measured environmental change Δf to the value which is inversely proportional to the Q-factor.

As a result, we will have the fiber-optical line with the number of sensor heads based on microvibrated fiber tips, it could be useful very much, for example as a kind of chemical sensors [9] to control pollution in a water and air. Multi-component, simple remote sensor system could be created in a near future. This method has following advantages: very small response time, high sensitivity and noise immunity.

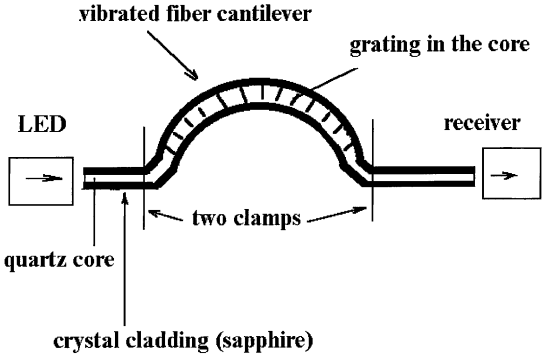

Fig. 2. Scheme of vibrations in case of two-clamped fiber section.

2. Amplitudes of vibrations

(a) Theoretical analysis was performed for vibrated fiber cantilever with a circular cross-section. The distributed driving force and the displacement were described by harmonic functions of time. The classical approach for description of the local amplitude was taked from [10]. Three equations for vibration amplitude are developing here. These equations correspond to the transverse vibrations of fiber tip [11], fiber cantilever with both clamped ends and longitudinal tip vibrations [12].

The cross-section vibrations of the cylindrical shape cantilever are described by equation from [10]

$$EJ\frac{\partial^4 W}{\partial x^4} + \rho F\frac{\partial^2 W}{\partial t^2} = P(x,t) \tag{1}$$

where ρ, F are the material density and cross-section area of the fiber, E the cantilever elasticity module, $W(x,\ t)$ the transverse displacement of the cantilever, t the time, $F = \pi R^2$ is a fiber cross-section, and the moment of inertia is $J = \pi R^4/4$, r the radius and L the whole length of vibrated fiber fragment and $P(x,t) = q\exp(\mathrm{i}\omega t)$ is the external force which causes this vibrations. The solution of this equation for tip is

$$\begin{aligned} W(\xi) = {} & -K + \frac{K}{2}[\cosh(\xi\alpha) + \cos(\xi\alpha)] \\ & + \frac{K}{2}\frac{\sinh(\alpha)\sin(\alpha)}{1+\cosh(\alpha)\cos(\alpha)}[\cosh(\xi\alpha) - \cos(\xi\alpha)] \\ & - \frac{K}{2}\frac{\sinh(\alpha)\cos(\alpha) + \sin(\alpha)\cosh(\alpha)}{1+\cosh(\alpha)\cos(\alpha)} \\ & \times [\sinh(\xi\alpha) - \sin(\xi\alpha)] \end{aligned} \tag{2}$$

where $W(\alpha\xi)$ is the transverse displacement along the dimensionless tip length $\xi = x/L$, and force parameter is $K = q/\omega^2\rho F$, it is transformed from the right part of Eq. (1). The next Eq. (3) is the result of the solution from appropriate boundary conditions

$$\cosh(\alpha)\cos(\alpha) = -1 \tag{3}$$

where $\alpha_1 = 1.8751$ for the first mode of mechanical vibrations, but $\alpha_2 = 4.6941$ for the second mode; but for higher modes $k > 2$ the f_k could be found with $\alpha_k = (2k-1)/2$. The resonance frequency of vibrations could be calculated according to the next equation

$$f_k = \frac{\alpha^2 r\sqrt{E}}{4\pi L^2\sqrt{\rho}} \tag{4}$$

The amplitude of vibrations at exact resonance frequency is limited by the fiber material property. It is an inner friction of material ψ which is inversely proportional to the Q-factor. In standard technique in represented in imaginary part of the Young module $\hat{E} = E(1 + \mathrm{i}\psi)$, α changes to $\hat{\alpha}$ in (2) and (3). The procedure of this analysis was fully in [11]. Based on this method, we present here the result equations for the real amplitude calculation of the transverse displacement $|\hat{W}(\zeta)|$

along the current axial coordinate ξ

$$\mathrm{Re}(\hat{W}(\alpha\zeta)) = K\left\{-1+\frac{1}{2}[\cosh(\alpha\zeta)+\cos(\alpha\zeta)]\right\},$$

$$\begin{aligned}\mathrm{Im}(\hat{W}(\hat{\alpha})) = {} & \frac{K\alpha\pi}{4Q}\zeta[\sinh(\alpha\zeta)-\sin(\alpha\zeta)] \\ & + \frac{KQ}{\alpha\pi}\frac{\cosh(\alpha)+\cos(\alpha)}{[\sin(\alpha)+\sinh(\alpha)]^2} \\ & \times\{[\sin(\alpha)+\sinh(\alpha)][\cosh(\alpha\zeta)-\cos(\alpha\zeta)] \\ & -[\cos(\alpha)+\cosh(\alpha)][\sinh(\alpha\zeta)-\sin(\alpha\zeta)]\} \quad (5)\end{aligned}$$

Calculated amplitudes are few microns for tip with length of about 1 mm and radius 30–62.5 μm are in agree with experimental ones. Calculations of the modulated optical power coincides with the experimental values which are 20–50 mW excitation power for vibrations of the fiber tips with the lengths amount 2 mm [1,4].

(b) Vibrated fiber fragment with both clamped ends differs from the case mentioned above by the equality of the boundary conditions at both clamped ends. Using this conditions we obtain the next Eq. (6) for displacement $W_2(\xi)$

$$\begin{aligned}W_2(\xi) = {} & -K+\frac{K}{2}[\cosh(\alpha\xi)+\cos(\alpha\xi)] \\ & + \frac{K}{2}\frac{\cosh(\alpha)-\cos(\alpha)-\sin(\alpha)\sinh(\alpha)}{1-\cosh(\alpha)\cos(\alpha)} \\ & \times[\cosh(\alpha\xi)-\cos(\alpha\xi)]+\frac{K}{2} \\ & \times\frac{\sinh(\alpha)\cos(\alpha)-\sinh(\alpha)+\sin(\alpha)\cosh(\alpha)-\sin(\alpha)}{1-\cosh(\alpha)\cos(\alpha)} \\ & \times[\sinh(\alpha\xi)-\sin(\alpha\xi)] \quad (6)\end{aligned}$$

This vibrated fragment has resonance when the denominator is about zero that occurs when $\alpha_1 = 4.7300$ with the same (3). Following the analogous procedure for $|\hat{W}_2(\zeta)|$ calculation we have appropriate equations for the real amplitude. We use here simplified Eq. (7), because only the imaginary part of amplitude equation considerable increase during the resonance

$$\begin{aligned}|\hat{W}_2(\zeta)| \approx {} & \frac{KQ}{\alpha\pi}\left\{[\cosh(\alpha\zeta)-\cos(\alpha\zeta)]\frac{\sinh(\alpha)\sin(\alpha)-\cosh(\alpha)+\cos(\alpha)}{\sin(\alpha)-\sinh(\alpha)}+[\sinh(\alpha\zeta)-\sin(\alpha\zeta)]\right. \\ & \left.\times\frac{\sin(\alpha)\sinh(\alpha)[\cosh(\alpha)-\cos(\alpha)]-[\cosh(\alpha)+\cos(\alpha)]^2}{[\sinh(\alpha)-\sin(\alpha)]^2}\right\} \quad (7)\end{aligned}$$

For all vibration calculations of this paper, we use the following quartz parameters: $E = 73\times10^9$ Pa, $\rho = 2.2\times10^3$ kg/m^3, Q-factor of mechanical vibrations is $Q = 2400$. The force per one unit of fiber length in case of tip deviation was $q = 10^{-2}$ N/m in Eqs. (1) and (2) and below. Results of the amplitude calculations according to (7) are shown in Fig. 3. The amplitude at the middle fiber fragment is small as $W_2 = 7.18$ μm for a quartz fiber with $R = 62.5$ μm and $L = 5$ mm, and $W_2 = 149.13$ μm when $L = 10$ mm. For tip vibrations this amplitude is higher according Eqs. (1)–(5). Typical amplitudes of vibrations and fiber fragment with both clamps are shown in Fig. 3.

(c) At last, we consider the longitudinal vibrations. There are another possibility of the fiber oscillations without bending of its tip. In this case, the direction of vibrations coincides with the axes of optical-fiber. Amplitude of such vibrations is calculated according to the procedure from [12] and in resonance is given by next equation

$$\begin{aligned}& U(\zeta) = \sqrt{\varphi^2(\zeta)\sin^2(\omega t)+\gamma^2(\zeta)\cos^2(\omega t)}, \\ & \varphi(\zeta) = C\sinh(\alpha_1\zeta)\cos(\alpha\zeta)-D\cosh(\alpha_1\zeta)\sin(\alpha\zeta), \\ & \gamma(\zeta) = D\sinh(\alpha_1\zeta)\cos(\alpha\zeta)+C\cosh(\alpha_1\zeta)\sin(\alpha\zeta) \\ & \alpha_1 = \left[-\frac{\sqrt{(\beta_1^4+\mu_2^2)(1+\mu_1^2)}-(\beta_1^2-\mu_1\mu_2)}{2(1+\mu_1^2)}\right]^{1/2}, \\ & \alpha = \left[\frac{\sqrt{(\beta_1^4+\mu_2^2)(1+\mu_1^2)}+(\beta_1^2-\mu_1\mu_2)}{2(1+\mu_1^2)}\right]^{1/2}, \\ & k_1 = \cosh(a_1)\cos(a)+\sinh(a_1)\sin(a), \\ & k_2 = \cosh(a_1)\cos(a)-\sinh(a_1)\sin(a), \\ & \mu_1 = \frac{\chi_1\omega}{FE}, \qquad \mu_2 = \frac{\chi_2\omega L^2}{FE}, \\ & C = \frac{K[k_1(\mu_2 a-a_1)+k_2(\mu_2 a_1-a)]}{(a_1^2+a^2)[\cos^2(a)+\sinh^2(a_1)](1+\mu_2^2)}, \\ & D = \frac{K[k_1(\mu_2 a_1+a)+k_2(\mu_2 a+a_1)]}{(a_1^2+a^2)[\cos^2(a)+\sinh^2(a_1)](1+\mu_2^2)} \quad (8)\end{aligned}$$

where χ_1 and χ_2 are the inner and external attenuation coefficients, $\beta = \omega L\sqrt{\rho}/\sqrt{E}$ the frequency parameter as α in the case of transverse vibrations. For the first vibration mode $\beta_1 = \pi/2$, and K the force parameter. Resonant amplitude of the longitudinal vibrations of the tip end with the length $L = 5$ mm is $U(L) = 7.18$ μm according calculations from (8), which is by 50 times smaller than it's bend amplitude at the same conditions. But this method attaches importance for deformations in the middle fiber axis where Bragg-grating is located, so we will begin analysis this deformation due through this vibrated amplitudes.

3. Deformations in a fiber during deviation

(a) Let us consider the elongation $\varepsilon_T(\xi, R)$ of the fiber tip at it's bend position during vibration, this term means small

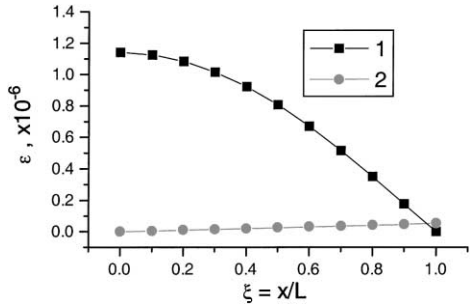

Fig. 3. Amplitudes of vibrations $|W(\xi)|$. Curve 1 corresponds to the tip with $L = 5$ mm, $2R = 125$ μm; Curve 2 corresponds to vibrated fiber with both clamped ends ($L = 10$ mm and the same radius).

local increase of the length of fiber cantilever. According to the classical theory the force applied in transverse direction gives the bending elongation $\varepsilon_T(\xi, R)$. At first, let us consider the central axial line in a cylindrical fiber, because the Bragg-grating [11] is located in the central area of a fiber cross-section at distance of $h = 1$–3 μm from the central fiber axis. According to the linear theory of mechanics the transverse part of applied force do not causes the elongation of the central axial line in both bending tip as in two-side clamp fragment cases. The non-uniform function of the bend strain and appropriate elongation were found here through the distance h from the central fiber line and bending radius $r_c(\xi)$. This value $\varepsilon_T(\xi, R)$ is inversely proportional to the curvature radius of the bent optical-fiber and is calculated using the second derivative to the fiber displacement $W(\xi)$

$$\varepsilon(R, \xi) = \frac{h(R)}{r_c(\xi)} = h(R)W''(\xi) \tag{9}$$

The bending radius of curvature could be determined from displacement

$$\frac{1}{r_c(\zeta)} = \frac{M}{EJ}, \qquad \frac{1}{r_c(\zeta)} = W''(\zeta) \tag{10}$$

where $r(\xi)$ is the curvature radius of the bent optical-fiber, which varies along current axial coordinate ξ together with the function of displacement $W(\xi)$. Where h is the distance from the fiber axis in radial direction. The method of second derivative calculation $|\hat{W}''(\xi)|$ was the same one as for amplitude $|\hat{W}(\zeta)|$, so α was changed to corresponding complex value at exact resonance frequency. The approximate formula of $\varepsilon(\xi)$ could be achieved by comparison of all terms at exact resonance, but only the term which is multiplied to the value of Q-factor must be taking into account

$$\varepsilon(\xi, h) \approx h\,\mathrm{Im}[\hat{W}''(\xi)] \approx h\frac{KQ\alpha}{\pi}\{G[\cosh(\alpha\xi) + \cos(\alpha\xi)] + G^2[\sinh(\alpha\xi) + \sin(\alpha\xi)]\},$$
$$G = \frac{\cosh(\alpha) + \cos(\alpha)}{\sin(\alpha) + \sinh(\alpha)} \tag{11}$$

This approximate formula gives maximal descrepance from the exact values less than 1%. Approximate approach is more exact for the cantilevers made from materials with high Q-factor. The comparison of this bend elongation and longitudinal one was done at previous paper [11]. The longitudinal kind of tip elongation is exceed by this bend ones by 15–20 times of this bend ones for $h = 1$–3 μm for the equal forces of vibration excitation for short tip lengths, but, this difference is decreasing during increase of vibrated lengths.

(b) More simple physical model seems better for description of behavior of vibrated fragment with two clamped ends. At first, we represented such fiber as the arch during deviation. We could calculate the uniform inner elongation with the help of this model as follows:

$$\varepsilon_T = \frac{L_{arch}}{L_{line}} - 1 = \frac{r\varphi - L}{L} \approx \left[\left(\frac{L\arcsin(4W_{max}/L)}{4W_{max}}\right) - 1\right] \tag{12}$$

where r is the curvature radius of deviated fiber. For these cases we have appropriate average values of elongations, they are $\varepsilon = 7.2 \times 10^{-6}$; 1.15×10^{-4} for vibrated lengths $L = 5$ and 10 mm accordingly.

So, we can see below that the previous our approach as (9) is more preferable in comparison with (12) to find deformations in cross-section of vibrated fiber fragment with both clamped ends. But previous approach (9) could be applied also here because our typical amplitudes is more smaller than fiber radius. As it was done in (11) we get the value $|\hat{W}_2''(\xi)|$ from Eq. (7). With account of the inner friction of material and complex form of the Young's modules we get simplified elongation low for $\varepsilon_2(R, \xi)$

$$\varepsilon_2(\xi, h) \approx h\,\mathrm{Im}[\hat{W}_2''(\xi)] \approx h\frac{KQ\alpha}{\pi} \times \left\{ -[\sinh(\xi\alpha) + \cos(\xi\alpha)] \times \frac{\sinh(\alpha)\sin(\alpha) - \cosh(\alpha) + \cos(\alpha)}{\sinh(\alpha) - \sin(\alpha)} + [(\sinh(\xi\alpha) + \sin(\xi\alpha)] \times \frac{\sin(\alpha)\sinh(\alpha)[\cosh(\alpha) - \cos(\alpha)] - [\cosh(\alpha) + \cos(\alpha)]^2}{[\sinh(\alpha) - \sin(\alpha)]^2} \right\} \tag{13}$$

The results according to (13) for the elongation in vibrated fiber fragment are presented at Fig. 4. Calculations were done for three axial levels: at central neutral fiber axis $h = 0$, at the half of radius ($h = 30$ μm) and near the fiber surface at $h = 62.5$ μm. One can see the non-linear length increase other the coordinate ξ and this function has maximum at the middle of vibrated fiber.

In Fig. 4, the results of calculations are presented for this bend elongation. We see that this bending deformation is amount $\varepsilon_T \sim 10^{-7}$ to 10^{-8}, so it could be neglected in comparison with the elongation of whole fiber together with it's central axis deformations $\varepsilon_{arch} = 3.35 \times 10^{-5}$.

(c) We could consider a fiber length increase (and compression) during the longitudinal vibrations. The inner

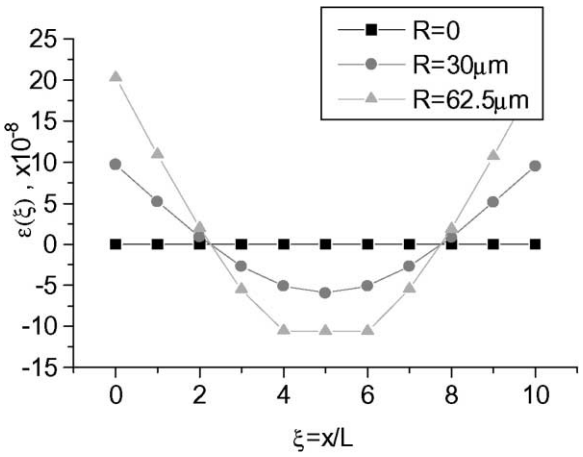

Fig. 4. Bend elongation in case of the both-side clamped fiber fragment with $L = 10$ mm, $2R = 125$ μm, (deformation was calculated at the distance $h = 0$, 30, and 62.5 μm from the central fiber axis).

vibrated fiber stress is determined through elongation as $\sigma = E\varepsilon$. This is important consideration for optimal operation of the tip Bragg-grating, $\varepsilon_L = (\partial U(\xi, t))/\partial\xi$.

This value could be found as the derivative of the displacement $U(\xi, t)$ from (8) at resonance. Tip stress [12] is maximal at the clamped end at $\xi = 0$ according to (9). The result equation is

$$\frac{\partial U}{\partial \xi} = \frac{\sqrt{2}K[\alpha_1 \sinh(\alpha_1\xi)\cosh(\alpha_1\xi) + \alpha \sin(\alpha\xi)\cos(\alpha\xi)]}{\sqrt[4]{(\beta_1^4 + \mu_2^2)(1+\mu_1^2)}\sqrt{(\sinh^2(a_1\xi) + \sin^2(a\xi))(\cos^2 a + \sinh a_1)}} \tag{14}$$

The non-uniform displacement $U(\xi)$ and appropriate non-uniform length increase were calculated for vibrated tip (see Fig. 5). This ε function is interesting for the operation of inner fiber grating. We will consider the different kinds of fiber deformations below in order to compare their influence to the fiber grating spectrum.

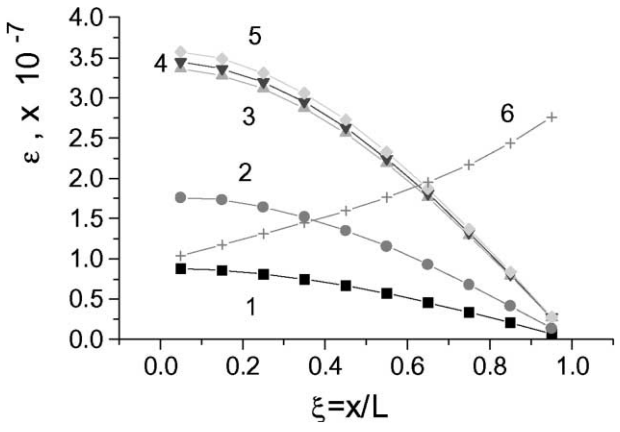

Fig. 5. Elongation functions in case of fiber tip longitudinal vibrations (curves 1–5). Parameters are: $R = 62.5$ μm; $L = 3.5$ mm (curve 1), 5 mm (curve 2). Curves 3–5 are for the tip with $L = 7$ mm in air (curve 5), pure water (curve 4) and in water with 1% of oil (curve 3). Graph 6 corresponds to the transverse tip vibration with $R = 62.5$ μm, $L = 7$ mm, and the same exciting force $q = 0.01$ N/m.

4. Fiber gratings to fix fiber vibrations

Grating filters in fiber core are very suitable and convenient to fix vibrated amplitude of fiber cantilevers. Wavelength reflected signal (or transmitted one) allows the absolute measurements and further processing.

Fiber grating can be created by standard holographic (or by mask) method in a core of a quartz fiber by ultraviolet irradiation. According to the applied periodical laser light intensity to the fiber core the plates with the different refractive indexes in quartz will be appear perpendicular to the fiber z axis

$$n(z) = n + \Delta n \cos\left(\frac{2\pi z}{\Lambda}\right) \tag{15}$$

At first we will consider the fiber Bragg-grating operation during vibrations. The main coupled waves equations for the waves considered according to matrix approach [8]

$$\frac{\mathrm{d}A(z)}{\mathrm{d}z} = kB\exp[\mathrm{i}(2\,\mathrm{d}\beta\, z - \varphi)],$$
$$\frac{\mathrm{d}B(z)}{\mathrm{d}z} = kA\exp[-\mathrm{i}(2\,\mathrm{d}\beta\, z - \varphi)] \tag{16}$$

$$\mathrm{d}\beta = \beta - \beta_{\mathrm{Bragg}} = \frac{2\pi n}{\lambda} - \frac{\pi}{\Lambda} \tag{17}$$

The electric fields of the backward and forward modes in this grating can be expressed as $E_{\mathrm{A}}(z) = A(z)\exp(-\mathrm{i}\beta z)$ and $E_{\mathrm{B}}(z) = B(z)\exp(-\mathrm{i}\beta z)$, respectively (see Fig. 6). Where β is the propagation constant in the fiber axis direction, and Λ the Bragg-grating constant. Where k is a coupling grating coefficient between forward and backward waves, $k = \pi\Delta n/\lambda$, this value could be varied in experiments by changing of fiber-core refractive index Δn by variation of UV-irradiation. Let us determine the $E_{\mathrm{A}}(0)$ and $E_{\mathrm{A}}(L)$ as the forward waves at the initial and last parts of the grating accordingly, and $E_{\mathrm{B}}(0)$, $E_{\mathrm{B}}(L)$ are the back waves in the grating at plates $z = 0$ and L. The grating reflection will be

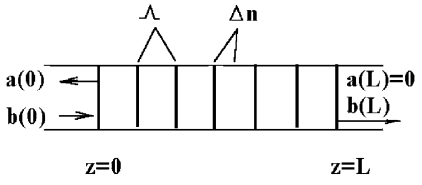

Fig. 6. Scheme of the waves propagated through the fiber grating.

$R = |F_{21}/F_{11}|^2$ by this approach from the appropriate transfer-matrix terms

$$\begin{pmatrix} E_A(0) \\ E_B(0) \end{pmatrix} = [F] \begin{pmatrix} E_A(L) \\ E_B(L) \end{pmatrix},$$

$$F_{21} = F_{12}^* = -kL \sinh(\gamma L) \exp \frac{\mathrm{i}(\beta_B L + \varphi)}{\gamma L},$$

$$F_{12}^* = F_{11} = \left[\cosh(\gamma L) + \frac{\mathrm{i}\, \mathrm{d}\beta\, L \sinh(\gamma L)}{\gamma L} \right] \exp(\mathrm{i}\beta_B L),$$

$$\gamma = \sqrt{k^2 - (\mathrm{d}\beta)^2} \tag{18}$$

Now let us consider the changes of one elemental gratings. Bragg-grating spectral change is due to the deformations of the fiber length during cantilever deviation: $L \Rightarrow L(1 + \varepsilon)$. Also this changes acts to the grating constants

$$\Lambda = \Lambda_0(1 + \varepsilon_N) \tag{19}$$

On the other hand, the coupling coefficient varies along the tip (and differs from one of non-stretched grating k_0), it must be changed during tip stretching due to deviation because quartz refractive index (as n as Δn in (15)) is a function of the strain [7]

$$\frac{n(z)}{n} = 1 - 0.5n^2[p_{12} - \nu(p_{11} + p_{12})]\varepsilon_N = 1 - \chi\varepsilon_N,$$

$$\chi \approx 0.21 \tag{20}$$

The fiber photoelastic constants are $p_{11} = 0.112$, $p_{12} = 0.252$, and $\nu = 0.17$ is Poisson's ratio.

Let us make the next additional introduction of the ε-function into the main equation at each Nth grating segment

$$k \Rightarrow k_{\varepsilon=0} + C_1\varepsilon_N, \qquad C_1 = -\frac{\pi\chi\,\Delta n_N}{\lambda},$$

$$\mathrm{d}\beta \Rightarrow \mathrm{d}\beta_{\varepsilon=0} + C_2\varepsilon_N, \qquad C_2 = \frac{\pi(1-\chi)}{\Lambda_N},$$

$$\gamma \Rightarrow \gamma_{\varepsilon=0} + C_3\varepsilon_N \tag{21}$$

In this work, the matrixes approach [8] was improved to account fiber deformations described above. It allowed to calculate the result in case of strong non-linearity function what is considerable circumstance for fiber tip or fragment with $L = 1$–10 mm. We divided of whole grating into N small segments, and in every one the coupled mode equations could be utilized to describe the contradirectional coupled wave interaction by the Riccati differential equations.

Whole grating will be described as a final matrix multiplication of all elemental matrixes of segments

$$\begin{pmatrix} E_A(0) \\ E_B(0) \end{pmatrix} = [F_1][F_2] \cdots [F_N] \cdots [F_L] \begin{pmatrix} E_A(L) \\ E_B(L) \end{pmatrix} \tag{22}$$

Each segment can be assumed to be uniform but to have it's own values of k, Λ, and n that slightly differs from it's neighbors. Thus, we represent a grating with the total length L in vibrating fiber cantilever as a cascade of several small uniform gratings. Each segment is treated as a uniform grating with its own F-matrix.

π-phase shifted fiber Bragg-gratings was considered in this paper as a good method to measure vibrations of the fiber tips with the lengths of several millimeters. Its spectral half width near resonance is thinner, as it could be for usual Bragg-grating. Let us consider the π-shifted Bragg-grating in the fiber tip as two parts with the π-phase difference in the middle of the grating, which is the center of the fiber cantilever. At first let us divide the tip and the grating into two halfs according to length, so first part has length from 0 up to $\xi = 0.5$ at the horizontal axis and second part appropriates to $0.5 < \xi < 1$. Both first and second half of this cantilever were calculated with the help of the software created according to method described above. During the multiplication of this result matrixes the wave phase $\varphi_1 = 0$ for the first $N/2$ elementary gratings, but $\varphi_2 = \pi$ was the initial phase for the second half of grating segments with numbers from $N/2$ up to N. The final matrix is appropriate to such grating is the result of multiplication of two-half of matrixes of both grating parts by software.

5. Results of calculations of π-shifted Bragg-grating

In the figures below you can see the spectrums of π-shifted Bragg-grating which were calculated under the different sets of initial data. These results were calculated using software developed for this problem. The longitudinal vibrations of fiber tip is interesting very much for as high-sensitive sensor for environment [12], also the future practical utilization in [14]. These spectrums are shown over $\mathrm{d}\beta$ at Figs. 7–12. The $\mathrm{d}\beta$ is variable change of the propagation constant from it's Bragg condition, it could be recalculated using the wavelength

$$\mathrm{d}\beta = \frac{2\pi n\, \mathrm{d}\lambda}{\lambda_{\mathrm{Bragg}}^2} \tag{23}$$

here $\mathrm{d}\lambda$ is change of the wavelength from it's Bragg condition. Complete reflection spectrum of the π-shifted

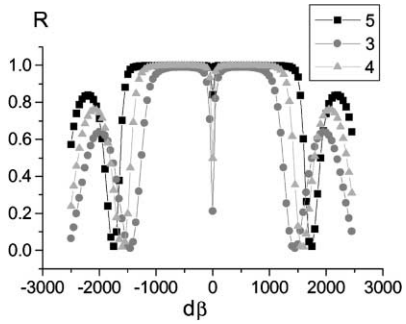

Fig. 7. Complete reflection spectrum for the π-shifted Bragg-grating with central narrow band. Grating parameters are: $L = 5$ mm, $R = 62.5$ μm, curves 3–5 are correspond to $\Delta n = 3 \times 10^{-4}$; 4×10^{-4}; and 5×10^{-4}, respectively.

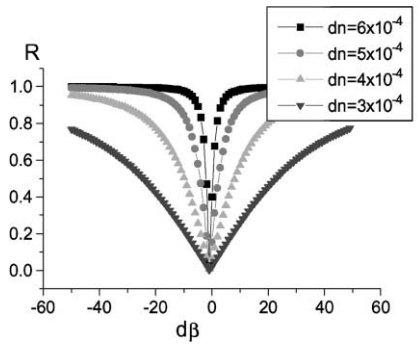

Fig. 8. More detailed reflection spectrum central band for the π-shifted Bragg-grating. Grating parameters are: $L = 5$ mm, $R = 62.5$ μm, elongation function used is shown in Fig. 4 (curve 2), Δn varied from 3×10^{-4} to 6×10^{-4}.

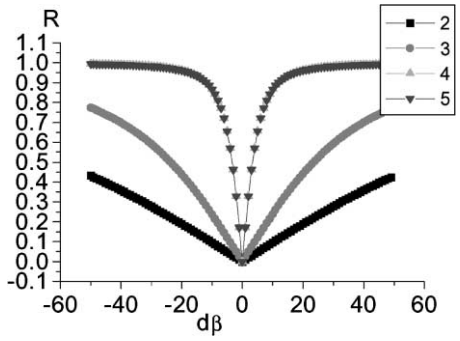

Fig. 9. Reflection spectrum of π-shifted Bragg-grating. Grating parameters are: $L = 5$ mm, $R = 62.5$ μm, elongation $\varepsilon = 0$, Δn varied from 2×10^{-4} to 5×10^{-4} (curves 2–5, respectively).

Bragg-grating which includes the central narrow band and two-side grating second orders of reflection shown in Fig. 7. Grating parameters are: $L = 5$ mm, $R = 62.5$ μm, Bragg wavelength $\lambda_{\text{Bragg}} = 1.3$ μm. More detailed central band of reflection spectrum of the π-shifted Bragg-grating shown in Fig. 8. Grating parameters are: $L = 5$ mm, $R = 62.5$ μm.

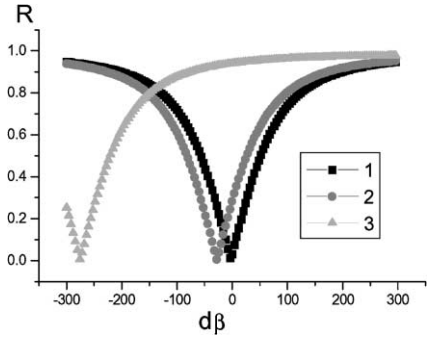

Fig. 10. π-Shifted grating reflection spectrum (longitudinal vibrations). Grating parameters are: $L = 3.54428$ mm, $R = 25$ μm, $\Delta n = 3.5 \times 10^{-4}$; spectrum 1 corresponds to the tip elongation shown in Fig. 4 curve 2. Spectrum 2 corresponds to the tip elongation 10 times greater than in spectrum 1 case. Spectrum 3 corresponds to the tip elongation 100 times greater than in spectrum 1 case.

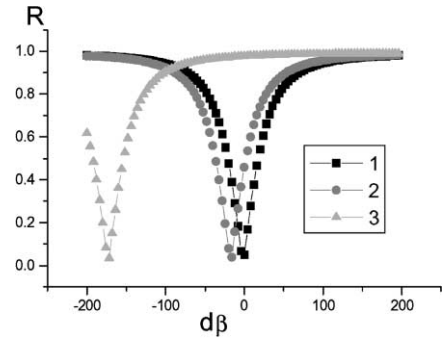

Fig. 11. Reflection spectrum of π-shifted Bragg-grating (longitudinal vibrations). Gratings parameters are: $L = 7.0$ mm, $R = 62.5$ μm, $\Delta n = 2 \times 10^{-4}$. Spectrum 1 corresponds to the tip elongation shown in Fig. 4 curve 5. Spectrum 2 corresponds to the tip elongation 10 times greater than in spectrum 1 case. Spectrum 3 corresponds to the tip elongation 100 times greater than in spectrum 1 case.

Elongation function was used in spectrum calculating according to the data from Fig. 5 and from the Eq. (13), dn was changed from 3×10^{-4} up to 6×10^{-4}. From this Fig. 8 one can see that the half-width of the central wavelength spectral band is sensitive to the grating coupling coefficient k, which is depending of the refractive-index change dn during grating UV-fabrication. One can calculate from the Fig. 8 that the half-width of the central wavelength spectral band is $\mathrm{d}\beta = 18\ \mathrm{m}^{-1}$ for the grating with $\Delta n = 4 \times 10^{-4}$, it's correspond to the wavelength half-width $\mathrm{d}\lambda = 3.3 \times 10^{-3}$ nm.

Fig. 9. shows the reflection spectrum of π-shifted Bragg-grating with the same parameters as in previous case, but without vibrations at elongation $\varepsilon = 0$. Grating parameters are: $L = 5$ mm, $R = 62.5$ μm, Δn was changed from 2×10^{-4} up to 5×10^{-4} (curves 2–5, respectively). The spectral band (at Fig. 9) is $\mathrm{d}\beta = 7\ \mathrm{m}^{-1}$ for the grating with $\Delta n = 4 \times 10^{-4}$. By comparison of Figs. 8 and 9 we see that grating has enough sensitivity to recognize vibration elongation as $\varepsilon \approx 10^{-7}$ because appropriate spectral half-width

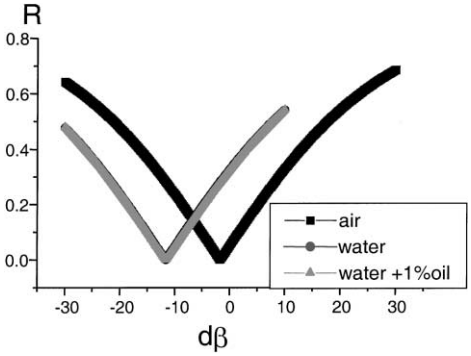

Fig. 12. Reflection spectrum of π-shifted Bragg-grating (transverse vibration). Gratings parameters are: $L = 7.0$ mm, $R = 62.5$ μm, $\Delta n = 2 \times 10^{-4}$. Spectrum 1 corresponds to the tip elongation shown in Fig. 4 curve 6. Spectrum 2 corresponds to the tip elongation 10 times greater than in spectrum 1 case. Spectrum 3 corresponds to the tip elongation 100 times greater than in spectrum 1 case.

differs from each other considerably, so is $d\lambda_{1/2} = 3.32 \times 10^{-3}$ nm at Fig. 8 and $d\lambda_{1/2} = 1.29 \times 10^{-3}$ nm at Fig. 9, therefore, their difference is $\delta(d\lambda_{1/2}) = (3.32 - 1.29) \times 10^{-3}$ nm $= 2.03 \times 10^{-3}$ nm.

The next Figs. 10 and 11 show π-shifted grating sensitivity to the grating length. The graph 1 at Figs. 10 and 11 represents the grating spectrum with account of elongation function ($\varepsilon_1 \sim 10^{-7}$) shown in Fig. 5. The graphs 2 represent the elongation which is increased 10 times ($\varepsilon_2 \sim 10^{-6}$); and graph 3 represents elongation which is increased by 100 times $\varepsilon_3 \sim 10^{-5}$. These increase of elongation ε_2, ε_3 are the simple result of appropriate increase of the force of vibration excitation in Eq. (1) by 10 and by 100 ($P_3 = 100P_1$). We can see in Fig. 10 that ever short ($L = 3.5$ mm) π-shifted grating could detect the increase of elongation with enough sensitivity. Comparing Figs. 10 and 11 we see that more longer grating gives more narrowing of the central spectral band.

Fig. 12 shows calculated grating spectrum with account of elongation during transverse vibrated cantilever, which is presented at graph 6 of the Fig. 5. By comparison of Figs. 11 and 12 one can see that grating spectrum has no considerable difference for longitudinal and transverse kind of vibrations for approximately equal values of vibration elongation.

Fig. 13 shows the π-shifted grating operation under the water (graph 2) and under the dirty (viscous) water with 1% of dissolved oil (graph 3). It is known from the classical mechanics that the amplitudes of longitudinal vibrations are sensitive to the external medium friction and mainly depend on the viscosity of surrounding medium. This calculations show that such grating can measure the viscosity of the surrounding media very well. Grating parameters are: $L = 7.0$ mm, $R = 62.5$ μm, $\Delta n = 2 \times 10^{-4}$. Graph 1 represents the tip elongation in air with the values of elongation $\varepsilon \sim 10^{-5}$. During calculations of the graphs 2 and 3, we used another elongation functions that were calculated according

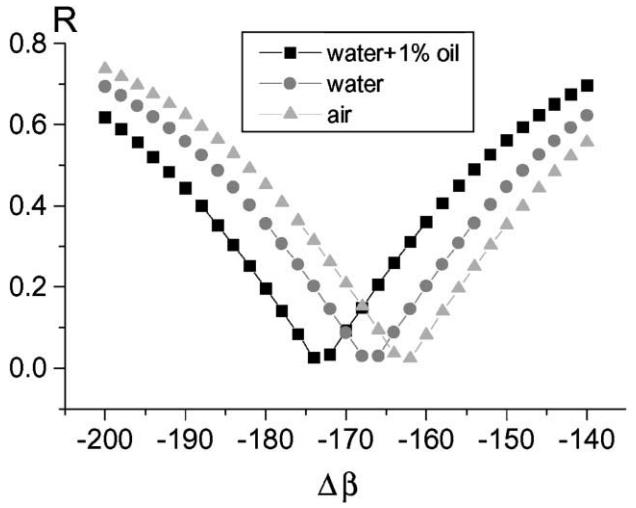

Fig. 13. Reflection spectrum of π-shifted Bragg-grating. Gratings parameters are: $L = 7.0$ mm, $R = 62.5$ μm, $\Delta n = 2 \times 10^{-4}$; these spectrums correspond to the tip in the air, water and water with 1% of oil (elongation is 100 times greater than that shown in Fig. 4 curves 3–5).

to Eq. (14) and method described in [12] with account of the real different external media such as air, water and dirty water + 1% oil (see parameters α and α_1 in [12]). For air viscosity was chosen $\mu_{air} = 0.18 \times 10^{-4}$ Pa s; for pure water $\mu_{water} = 1.14 \times 10^{-3}$ Pa s; and for dirty water $\mu_{mix} = 1.97 \times 10^{-3}$ Pa s as a mixture of the pure water value with 1% of viscosity of pure oil ($\mu_{oil} = 0.083$ Pa s). This difference of the viscosity of surrounding media is resulted in the appropriate functions of elongation during this tip vibration. The band shifts for these three curves are $d\lambda_0 = 31.83 \times 10^{-3}$ nm (air), $d\lambda_0 = 30.73 \times 10^{-3}$ nm (water), $d\lambda_{1/2} = 30.36 \times 10^{-3}$ nm (water + 1% of oil). Graphs 1–3 are correspond to the strong values of tip elongation ($\varepsilon_3 \sim 10^{-5}$) so this values of elongation are multiplied to 100 in comparison with the curves 3–5 at Fig. 5.

The results at Figs. 7–12 are performed for vibrated fiber tips with parameters used in the set of experiments, length $L = 3$–7 mm and typical several microns of vibrated amplitude. The calculated changes in this grating spectrum are based on the deformations in vibrated fiber tip. π-Shifted Bragg-grating has high sensitivity to measure these typical fiber vibrations.

6. Alternative long-period gratings

Long-period grating that couple the fundamental mode to different forward propagating cladding modes have been demonstrated. This coupling to the cladding mode is highly selective. As a result, any modulation of the core and cladding guiding properties modifies the spectral response of long-period gratings, and this phenomena can be used for high sensitive measurement of the fiber deviations. In comparison with Bragg-grating which deals with fundamental mode placed in the fiber core this long-period one deals with high-order cladding modes which distributed almost uniformly into the whole area of fiber cross-section. These fiber cladding modes are localized in whole cladding cross-section with radius $R = 62.5$ μm, which is important for an operation of long-period gratings [13]. This grating fabricated by mask-method with UV laser radiation. The transmission spectrum of the long-period grating usually measured. The discrete spiky loss bands correspond to the coupling of the fundamental guided mode to discrete cladding mode. The matrix approach based on the coupling modes theory what describes the interaction of the core $R(z)$ and the cladding $S(z)$ modes in a single long-period grating gives the following equation [13] for the transmission amplitude

$$S(L)S^*(L) = \frac{k^2}{k^2 + \delta^2} \sin^2(L\sqrt{k^2 + \delta^2}),$$
$$\delta \approx \frac{2\pi}{\Lambda}\frac{\Delta\lambda}{\lambda} \tag{25}$$

where typical grating constant $\Lambda = 320$ μm, $\lambda = 1.3$ μm, $k = \pi\Delta n/\lambda$ is the grating coupling coefficient where change

of refractive index due to the UV-irradiation is $\Delta n = 0.015$ [13]. From previous equation we could find the next low (26) with account of (21) than deformation exist

$$S(L)S^*(L) \approx \sin^2\left[Lk + \frac{\delta^2 L}{2k}\right] \approx \sin^2\left\{kL + \frac{\delta^2 L}{2k} + \varepsilon\left[Lk(1-\chi) + \frac{\delta^2 L}{2k}(\chi - 1)\right]\right\} \quad (26)$$

For the center of the band at transmission spectrum (at $\delta = 0$) we will get more simple equation

$$SS^* \approx \sin^2\{kL + \varepsilon kL \times 0.79\} \quad (27)$$

Typical elongation is $\varepsilon = 1.15 \times 10^{-4}$ from previous calculations according (12) for length $L = 10$ mm, and values $kL = 365$ is really and could be use for further estimations. So, one can see from (30) that transmission $SS^* \approx 0.296$ at $\varepsilon = 0$, it's change up to $SS^* \approx 0.327$ at $\varepsilon = 1.15 \times 10^{-4}$, such intensity difference is 3.1%, which is high enough for the real experimental detection of vibrated fiber fragment.

The long-period grating could be successfully used for detection of vibrations of fiber section, the resonant frequency in amount kHz, and amplitude of vibrations is amount $W \sim 100$ μm.

7. Conclusion

Fiber-optic inner core gratings are considered together with the no uniform deformations which appear along oscillated optical-fiber. Analysis was done for vibrated fiber cantilevers with the length 1–10 mm, the resonant frequency is amount kHz, and amplitudes of vibrations are from 1 up to 100 μm. Different cases are analyzed which correspond to transverse or longitudinal vibrations of the fiber tips or fragments with two clamps. As π-shifted Bragg-grating as long-period grating could be successfully used for detection of vibrations of this fiber section.

References

[1] S. Inaba, H. Kumazaki, K. Hane, Photothermal vibration of fiber core for vibration-type sensor, Jpn. J. Appl. Phys. 34 (1995) 2018–2021.
[2] K.E.B. Thornton, D. Uttamchandani, B. Culshaw, A sensitive optically excited resonator pressure sensor, Sens. Actuators A 24 (1990) 15–19.
[3] N. Furstenau, M. Shmidt, H. Horack, W. Goetze, W. Schidt, Extrinsic Fabry–Perot interferometer vibration and acoustic sensor systems for airport ground traffic monitoring, IEE Proc.-Optoelectron. 144 (1997) 134–144.
[4] H. Kumazaki, S. Inaba, K. Hane, Temperature characteristics of vibrating type sensor using micromachined optical fiber-tip, Optic. Rev. 3 (1996) 135–138.
[5] W.B. Spillman Jr., D.R. Huston, Scaling and antenna gain in integrating fiber-optic sensors, J. Lightwave Technol. 13 (1995) 1222–1230.
[6] S. Huang, M.M. Ohn, M. LeBlanc, R. Lee, R.M. Measures, Fiber optic intra-grating distributed strain sensor, SPIE Proc. 2294 (1994) 81–92.
[7] M.A. Davis, A.D. Kersey, T.A. Berkoff, D.G. Bellemore, Subcarrier based path-integrating strain sensor array utilizing fiber Bragg-gratings, SPIE Proc. 2294 (1994) 93–99.
[8] M. Yamada, K. Sakuda, Analysis of almost-periodic distributed feedback slab waveguides via a fundamental matrix approach, Appl. Optics 26 (1987) 3474–3478.
[9] A.L. Popov, T.V. Tulaikova, Chemical sensor using fiber optic micromechanical vibrations, Transducers'95 Eurosensors XI, Stockholm, Sweden, 1995, pp. 437–440.
[10] A.P. Filippov, Vibrations of the Deformed Systems, Mashinostroenie, Moscow, 1970, p. 734.
[11] T.V. Tulaikova, A.I. Paskhin, R.R. Karle, S.R. Amirova, Analysis of the sensitivity of vibrating fiber-optic diffraction-grating sensors, Laser Phys. 10 (2000) 927–931.
[12] T.V. Tulaikova, Vibrated fiber optical sensors, analyze of the possibilities, Proc. SPIE 3781 (1999) 226–234.
[13] E.M. Dianov, S.A. Vasiliev, A.S. Kurkov, O.I. Medvedkov, V.N. Protopopov, Fiber Mach-Zender Interferometer Based on a Pair of Long-Period Gratings, ECOC-96, MoB.5.6, Oslo, Norway, 1996.
[14] P.K. Wei, W.S. Fann, The probe dynamics under shear force in near-field scanning optical microscopy, J. Appl. Phys. 83 (1998) 3461–3468.

Biographies

Gennadiy Gurchonok is postgraduate student of the Moscow Institute of Physics and Technology. He graduated from the Moscow Institute of Physics and Technology with honors in 2000. He was born in 1978 in St. Petersburg. His main science interests are signal and image processing, control theory and computer based modeling.

Irena Djodjua is fourth year student of the Moscow Institute of Physics and Technology. She was born in 1980 in Georgia. She graduated from the school and entered Moscow Institute of Physics and Technology in 1997. Her science interests now are mathematics and sensors.

Svetlana Amirova is second year excellent student of the Moscow Institute of Physics and Technology. She was born in 1982 in Moscow region. She graduated from school with honors and was entered Moscow Institute of Physics and Technology with in 1999. Her science interests are mathematics and mechanics.

Tamara Tulaikova is senior researcher of the Institute for Problems in Mechanics of Russian Academy of Sciences. In 1985 she received the PhD degree from the General Physics Institute of Russia Academy of Sciences, where she worked in the science field of optics, lasers and sensors. Fiber-optic mode selection processes and diffraction grating mechanisms are the main fields of research. At the same time she solved some problems of interaction of laser beam with surface. Several kinds of fiber-optic sensors were developed under her guidance during last years including the chemical sensors based on fiber porous dyed polymer fragment and the sensor based on quartz fiber cantilever mechanical oscillations.